Insulator−Metal and Structural Phase Phenomena in $K_xBa_{1-x}CoS_2$ ($x < 0.07$)

M. C. Gelabert,[†,§] R. J. Lachicotte,[‡] and F. J. DiSalvo*[,†]

Department of Chemistry, Cornell University, Ithaca, New York 14853-1301, and Chemistry Department, River Campus, University of Rochester, Rochester, New York 14620

Received September 3, 1997. Revised Manuscript Received November 25, 1997

$K_xBa_{1-x}CoS_2$ was synthesized by a new technique using a closed vitreous carbon crucible. Single crystals prepared from materials of nominal composition $x = 0.2$ were found to have only modest substitution levels ($x \approx 0.07$) by microprobe and X-ray analysis. The substituted compounds crystallize in $P4/nmm$, $a = 4.557(1)$, $c = 8.957(2)$, $R_1 = 2.03\%$, and $wR_2 = 4.20\%$, as determined by single-crystal X-ray diffraction. Measurement of electrical resistivity by the van der Pauw method reveals a phase transition with hysteresis at about 170 K for cooling and 210 K upon warming, with semiconducting behavior above ($\rho \approx 10^{-2}$ Ω cm) and metallic-like behavior ($\rho \approx 10^{-3}$ Ω cm) below the transition. Magnetic susceptibility data show a second-order transition around 270 K, along with a first-order transition around 150−200 K that displays significant hysteresis. The transition at 270 K is probably due to the onset of antiferromagnetic order, whereas the transition at lower temperatures is associated with structural modifications. Low-temperature X-ray diffraction, from 300 to 100 K, of single crystals indicates tetragonal → monoclinic → triclinic symmetry shifts upon cooling through this temperature range, with corresponding superlattice formation.

Introduction

The crystal structure and properties of the Mott−Hubbard insulator, $BaCoS_2$, have been studied in detail.[1−3] $BaCoS_2$ crystallizes in a centered orthorhombic Bravais lattice which can be reduced to a primitive monoclinic cell. The structure is slightly distorted from that of tetragonal, metallic $BaNiS_2$, which contains NiS_5 square pyramids. These polyhedra are edge-connected to make $[NiS_{4/4}S]^{2-}$ sheets, with Ba^{2+} above and below the pyramids[4] (Figure 1). In $BaCoS_2$, the pyramids are distorted in the square plane to make, on average, rectangular CoS_4 bases. A fraction of $BaCoS_2$ single crystals appear to crystallize in the high-symmetry tetragonal structure; the differences between crystals are likely due to small variations in composition. The powder, on the other hand, is consistently monoclinic even with a sulfur vacancy concentration up to 10%, which appears to significantly affect the degree of monoclinic distortion.[3] Single crystals of $BaCoS_2$ display multiple superstructures that involve doubling of the in-plane lattice parameters.

Thermodynamically, $BaCoS_2$ is unstable below 850 °C; the reaction products must be quenched from high temperatures to obtain phase-pure material. Electrical resistivity measurements of $BaCoS_2$ indicate semiconducting behavior with an estimated activation energy of 0.07 eV. High-temperature magnetic susceptibility measurements suggest that the Co^{2+} ions undergo an antiferromagnetic ordering around 310 K with the value of the Co magnetic spin under some debate.[3,5] Refine-

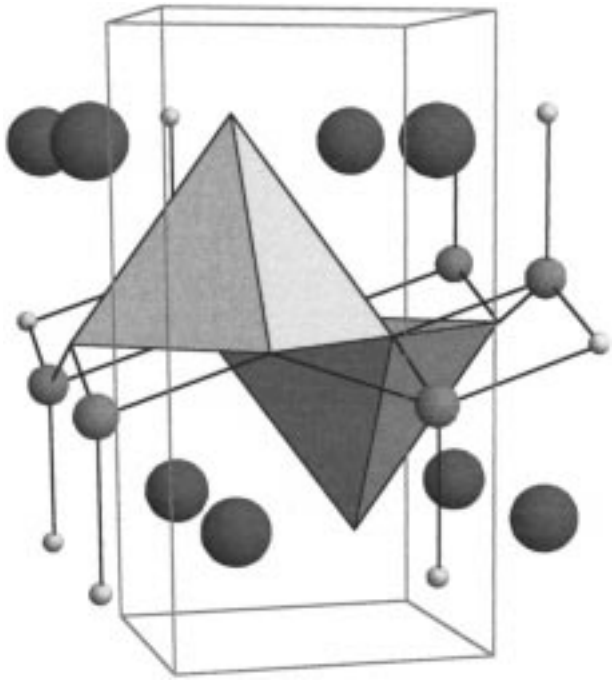

Figure 1. Approximate structure of $BaCoS_2$. The large spheres are Ba, medium Co, and small S. Square-pyramidal polyhedra represent CoS_5, which connect by the edges to form a sheetlike network.

* To whom correspondence should be addressed; (607) 255-7238; fjd3@cornell.edu.
† Cornell University.
‡ University of Rochester.
§ Current address: Department of Ceramic Engineering, Rutgers, the State University of New Jersey, Piscataway, NJ 08855.

(1) Snyder, G. J.; Gelabert, M. C.; DiSalvo, F. J. *J. Solid State Chem.* **1994**, *113(2)*, 355.
(2) Baenziger, N. C.; Grout, L.; Martinson, L. S.; Schweitzer, J. W. *Acta Crystallogr. C* **1994**, *50*, 1375.
(3) Gelabert, M. C.; Brese, N. E.; DiSalvo, F. J.; Jobic, S.; Deniard, P.; Brec, R. *J. Solid State Chem.* **1996**, *127(2)*, 211.
(4) Grey, I. E.; Steinfink, H. *J. Am. Chem. Soc.* **1970**, *92*, 5093.

S0897-4756(97)00604-2 CCC: $15.00
Published on Web 01/14/1998

ment of the structure from neutron diffraction data yields a Co spin of 3/2, with magnetic moments lying in the *ab* plane.[5] With magnetic susceptibility data, the value of the spin depends heavily on whether a temperature-independent susceptibility is included in the Curie−Weiss fit.

The structure of $BaCoS_2$, with distorted $CoS_{4/4}$ square sheets, is related to the $CuO_{4/2}$ sheets in the copper oxide superconductors. In the $CuO_{4/2}$ sheets half of the centers of squares formed by a two-dimensional square array of oxygen are filled by Cu; in $BaCoS_2$, all the squares are filled in by Co. The Cu d^9 spin $^1/_2$ state has been suggested to be an important criterion for superconductivity in the layered cuprate structures.[6] As mentioned above, the Co d^7 spin state in $BaCoS_2$ is still uncertain.

Some interesting work has been published over the last several years involving the substitution of $BaNiS_2$ and $BaCoS_2$. Martinson et al. reported insulator−metal transitions in sulfur-deficient, Ni-doped $BaCoS_2$.[7] In the $BaNi_xCo_{1-x}S_2$ alloys, resistivity and susceptibility measurements show a variation of properties with x. Like $BaNiS_2$, the Ni-rich side displays metallic behavior with Pauli paramagnetic susceptibility. For Ni concentrations less than 25%, the alloys are semiconducting, and their magnetic susceptibilities show broad transitions around room temperature, as observed in $BaCoS_2$. When sulfur vacancies are introduced to form $BaNi_xCo_{1-x}S_{2-y}$, the phases exhibit semiconducting behavior at high temperature and metallic, Pauli paramagnetic behavior at low temperatures, with a transition temperature around 200 K for $y = 0.2$, the maximum reported deficiency. Much additional work has evolved from the initial report, including detailed structure refinements,[8] Mössbauer experiments,[9] Hall effect,[10] thermoelectric measurements,[10] and high-pressure studies.[11]

The relatively small amount of reported work on chemical modification of $BaCoS_2$, combined with the interesting results thus far demonstrated with the $BaNi_xCo_{1-x}S_{2-y}$ system, warrants continued research on this unusual material. Substitution of Ba^{2+} by K^+ in $BaCoS_2$ is an appropriate choice since the ionic radii of both electropositive metals are comparable (1.35 and 1.33 Å for Ba^{2+} and K^+, respectively). The Fermi level (ϵ_F) would be shifted down in energy, since the total valence electron count decreases; on the other hand, doping with an electron donor, such as La^{3+}, would raise ϵ_F. In either case, the goal is to shift ϵ_F without disturbing the Co and S lattice, since these atoms largely determine the band structure near ϵ_F. Doping with K^+ would oxidize the CoS layers; the nature of oxidation (e.g., of Co, S, or both) depends on the primary band character at ϵ_F.

Here, we report the synthesis of $K_xBa_{1-x}CoS_2$ in closed vitreous carbon containers and describe the procedure for use of this crucible with reactive substances. Single crystals grown by this technique were characterized structurally with X-ray diffraction. Electrical and magnetic properties were measured and are reported.

Experimental Section

Synthesis. BaS was synthesized from the elements in dry liquid ammonia (Ba: 99.5+, S: 5N5) using a procedure similar to that for K_2S.[12] Two cobalt sulfides used as starting materials, Co_9S_8 and CoS_2, were both synthesized from the elements (Co: Alfa-Aesar 4N6, S: Metalspecialties 5N) in evacuated quartz tubes heated over 2−3 days to 600 °C. The Co metal was first reduced in a hydrogen stream at 600 °C; this treatment resulted in a small mass loss, presumably due to reduction of oxide. To minimize the potassium vapor pressure, K_2CoS_2[13] was used as the potassium source in these experiments. K_2CoS_2 was synthesized by reaction of equimolar amounts of K_2S (Cerac) and CoS (synthesized the same as Co_9S_8 and CoS_2) in a tightly covered vitreous carbon crucible. A 1-g charge was heated to 400 °C for 2 days and to 600 °C for 3 days and finally slow cooled with the furnace. The mass difference between reactants and products was negligible (≈2 mg). By X-ray powder diffraction, the product contained mostly K_2CoS_2 and some KCo_2S_2.[14] Presumably, the remaining potassium and sulfur was in the form of polysulfides. Even though this product was not single phase by X-ray diffraction, prereaction in this manner ensured that most or all of the potassium was contained in phases with vapor pressures lower than K_2S.

The early synthesis attempts for this particular substitution were fraught with problems including container attack and mass loss. The requirement that the material be heated to high temperatures (>850 °C), combined with a modest vapor pressure of K_2S which reacts with quartz and many container materials, makes the experimental challenges formidable. A new synthesis technique was developed to circumvent these problems. Vitreous carbon has all the chemical properties of polycrystalline graphite—stability and nonreactivity—without the undesirable porosity that limits its possible use as a tightly covered container.

Vitreous carbon crucibles were obtained along with matching, tapered caps. The cap and the crucible were carefully polished down to mirror-smooth surfaces with a slurry of silicon carbide or alumina powders (Buehler) and glycerol (Aldrich), finishing with a 0.05-μm grit. The crucible was placed in a quartz tube with glass wool, another smaller quartz tube, and a 200-g tungsten rod on top to provide extra force on the container lid (Figure 2). The tube was then sealed below the tungsten rod in the double-quartz area, in a manner that preserves the force exerted by the tungsten rod.

Stoichiometric quantities, corresponding to $K_{0.2}Ba_{0.8}CoS_2$ ($x = 0.20$), of the above starting materials were ground intimately, and the powder was pressed into a pellet of approximately 0.4 g. The reactants were sealed in the vitreous carbon container assembly under a little less than 1 atm of purified argon. The presence of inert gas in the tube improves the rate of quenching and suppresses potassium and sulfur loss, if the glassy carbon seal is not leaktight. The sealed quartz tube was heated to 840 °C over 12 h in vertical furnaces and held at that temperature for 3 days. The tube was subsequently quenched by dropping into an ice/water bath underneath the furnace.

(5) Mandrus, D.; Sarrao, J. L.; Chakoumakos, B. C.; Fernandez-Baca, J. A.; Nagler, S. E.; Sales, B. C. *J. Appl. Phys.* **1997**, *81(8)*, 4620.
(6) DiSalvo, F. J. In Nelson, D. L., Whittingham, M. S., George, T. F., Eds.; *Chemistry of High-Temperature Superconductors*; American Chemical Society: Washington, DC, 1987; p 49.
(7) Martinson, L. S. Schweitzer, J. W.; Baenziger, N. C. *Phys. Rev. Lett.* **1993**, *71(1)*, 125.
(8) Kodama, K.; Fujishita, H.; Harashina, H.; Taniguchi, S.; Takeda, J.; Sato, M. *J. Phys. Soc. Jpn.* **1995**, *64(6)*, 2069.
(9) Felner, I.; Gersten, J.; Litvin, S.; Asaf, U.; Kröner, T. *Phys. Rev. B* **1995**, *52(14)*, 10097.
(10) Takeda, J.; Kodama, K.; Harashina, H.; Sato, M. *J. Phys. Soc. Jpn.* **1994**, *63(10)*, 3564.
(11) Looney, C.; Schilling, J. S.; Martinson, L. S.; Schweitzer, J. W. *Phys. Rev. Lett.* **1996**, *76(25)*, 4789.
(12) Feher, F., In Brauer, G., Ed.; *Handbook of Preparative Inorganic Chemistry*; Academic Press: New York, 1963; p 360.
(13) Bronger, W.; Bomba, C. *J. Less Comm. Met.* **1990**, *158*, 169.
(14) Huan, G.; Greenblatt, M.; Croft, M. *Eur. J. Solid State Inorg. Chem.* **1989**, *26*, 193.

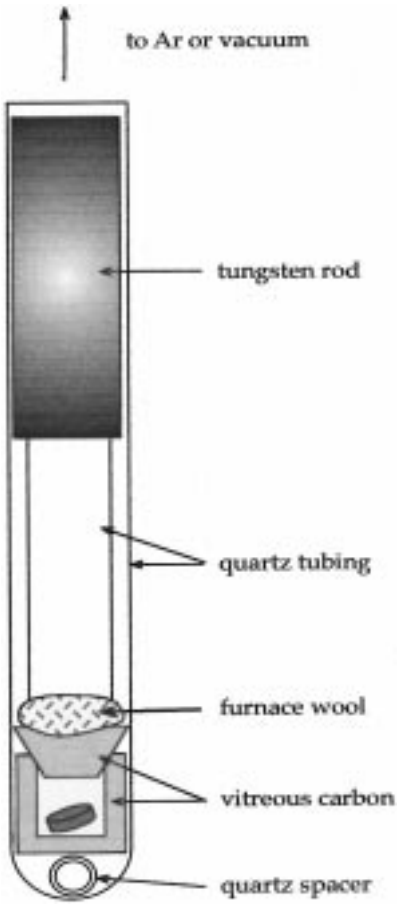

Figure 2. Quartz tube and vitreous carbon crucible assembly. After vacuum-pumping and filling the quartz with a specific amount of argon gas, the tube is sealed in the double-quartz area, at least 1 in. below the bottom of the tungsten rod.

The melted, black-gray product from this first heating was ground with a mortar and pestle, and heated to higher temperatures under one of two different conditions: closed and open vitreous carbon crucibles. With both regimes, the powder was placed into the crucible (open or closed) and sealed in quartz with about 1 Torr of purified argon. The samples were refired under several conditions; typically, the sealed quartz tubes were taken first to 950 °C over 12 h, kept at that temperature for 12 h, cooled over 48 h to 900 °C, and quenched immediately. The resulting products were black, with mixtures of polycrystalline powder and single-crystalline platelets of varying sizes, the largest of which were near 1 mm on an edge. The crystals were separated from the bulk sample manually after a light crushing with a mortar and pestle.

Scanning Electron Microscopy and Energy-Dispersive Spectroscopy. Scanning electron microscopy (SEM) coupled to a JEOL 733 Superprobe was utilized for identification and partial quantification of elements present in these crystals, as well as morphology inspection. The crystals were cleaned by scraping the surface with tweezers. Black platelets were mounted with carbon tape to a carbon stub and examined. Element identification and estimated element fractions of the crystal surface was obtained using energy-dispersive X-ray (EDS) standardless analysis.

Single-Crystal X-ray Diffraction. The black platy crystals obtained from the synthesis proved to be suitable for X-ray diffraction. A crystal was mounted on a glass fiber with Locktite Super Bonder and placed on the X-ray diffractometer. The X-ray intensity data were collected on a standard Siemens SMART CCD area detector system equipped with a normal focus molybdenum-target X-ray tube operated at 2.0 kW (50 kV, 40 mA). A total of 1.3 hemispheres of data was collected using a narrow-frame method with scan widths of 0.3° in ω and exposure times of 5 s/frame. Frames were integrated to 0.750 Å with the Siemens SAINT program, yielding a total of 916 reflections. The unit-cell parameters were based upon the least-squares refinement of three-dimensional centroids of 884 reflections. The space group was assigned on the basis of systematic absences and intensity statistics by using the program XPREP[15] (Siemens, SHELXTL 5.04). The structure was solved by direct methods (SHELXTL program, version 5.04) and refined by full-matrix least-squares on F^2. All atoms were refined with anisotropic thermal parameters, giving a data-to-parameter ratio of >10:1.

The crystal was then cooled in increments of 30 K. For each temperature, 20−70 reflection positions were used to index a unit cell. Lattice parameters were refined from 299 to 103 K. Below 183 K, there was a significant amount of distortion evidenced by split reflections and indexing difficulties. For two particular temperatures, 153 and 123 K, the SMART program had problems determining a unit cell from a large number of reflections. In these two cases, reduction to as few as 12 reflections was necessary in order to obtain a single unit cell.

Powder X-ray Diffraction. Single crystals (≈5 mg) were ground into a powder and placed into a sample holder. Powder X-ray diffraction patterns were taken with a Scintag XDS-2000 diffractometer with Cu Kα radiation. The reflection positions were determined with the Scintag peak-finder and deconvolution routines in the VMS software. Lattice parameters were refined using a locally written refinement code.

Electrical Resistivity. The temperature dependence of electrical resistivity was measured on a crystal of dimension $0.75 \times 0.40 \times 0.13$ mm^3. Four van der Pauw contacts were made with elemental indium to the corners of the rectangular plate using an ultrasonic soldering iron. Silver epoxy (Epotek) was used to make electrical connections from the contacts to four copper leads. Signal amplitude was measured using lock-in detection at a frequency of 23.0 Hz. Contact resistances were measured to be less than 50 Ω. The voltage−current characteristic was found to be linear over 4−20 mA, indicating ohmic contacts and a negligible capacitive or inductive contribution to the contact impedance.

Magnetic Susceptibility. Magnetic susceptibility was measured for $K_xBa_{1-x}CoS_2$ crystals from room temperature to 2 K. A SQUID magnetometer (Quantum Design MPMS), with a 7.5-T magnet, was used to make the measurements. About 5 mg of crystals (about 50−100) was separated from the product. The crystals were placed into a gelcap, which was then put into a soda straw sample holder. Because the crystals were platy, many of them were probably aligned with *c* parallel to the field lines. This complete assembly was lowered into the magnetometer. Sample signal was sufficient, evident from the integration of the paramagnetic peak signal as compared with the diamagnetic container. Due to the small quantity of sample, special care was taken to check the SQUID response at various temperatures, ensuring that the paramagnetic signal remained centered. The temperature dependence was measured twice at 2 T, with warming and cooling data being taken in the second run. Susceptibility vs field strength was measured at room temperature and at 2 K.

Results

Previous to crystal growth of $K_xBa_{1-x}CoS_2$, synthesis of polycrystalline powders of higher potassium content ($0.10 < x < 0.40$) was successfully accomplished with the closed container described. However, because the melting point of the powder dropped dramatically with increasing *x*, the temperatures appropriate for sintering pressed pellets were too low to stabilize the $BaCoS_2$ structure type. The melted products were suspected to be inhomogeneous and therefore not suitable for physi-

(15) Sheldrick, G. *Acta Crystallogr. A* **1990**, *46*, 467; *SHELXTL version 5 software*, Siemens Analytical X-ray Instruments, 1995.

Table 1. Lattice Constants of $K_xBa_{1-x}CoS_2$, As Determined by Powder X-ray Diffraction of Ground Crystals

material	*a* (Å)	*c* (Å)	*V* (Å^3)	γ
$K_xBa_{1-x}CoS_2$	4.547(2)	8.949(3)	185.0(1)	90
$BaCoS_2$ crystal[a,b]	4.568(1)	8.942(2)	186.6(1)	90
$BaCoS_2$ powder[b]	4.571(1)	8.938(1)	186.7(1)	90.5(1)

[a] Single-crystal X-ray diffraction values. [b] Data taken from previous work.[1,3]

cal measurements. These products, however, were single-phase by X-ray diffraction. The products annealed at lower temperatures contained Ba_2CoS_3 and CoS, the peritectoid decomposition products of $BaCoS_2$. Single crystals, then, proved to be the only suitable products for study.

The synthesis described here consists of two steps: reaction from powders and crystal growth via melt technique. Several attempts at crystal growth with the sealed crucible system for $0.1 < x < 0.4$ were done in order to minimize mass loss and therefore maximize substitution levels. Although these attempts did produce crystals large enough for measurement, preliminary EDS indicated that the potassium substitution for barium was <10 mol %, roughly independent of initial *x*. Furthermore, the crystals were too small to measure four-point resistance with indium contacts; other contact materials, such as silver paint and silver epoxy, were found to make unreliable contacts to this material. Growing crystals in an open container did not result in crystals with a significantly different composition. The crystals from open-container growth, however, were larger and morphologically ideal, and therefore were more suitable for resistance measurements.

Upon inspecting the quartz tubing after preliminary reaction, there were no signs of tube attack. The tubing was cloudy after reaction, but became clear after a mild heating in a flame, indicating that the cloudiness was due to a small amount of elemental sulfur condensed on the tube. The second heating for crystal growth also resulted in cloudy quartz, which in this instance was not due to elemental sulfur, but to quartz reaction with potassium. Some of the material had physically left the crucible due to the wetting of the container walls, resulting in melt flow out of the crucible. Therefore, a reliable measure of mass loss could not be determined in this case.

The powder X-ray diffraction pattern was similar to that of $BaCoS_2$, but did not display the 11*l* splitting associated with a distortion to a monoclinic primitive cell.[3] Lattice parameters are listed in Table 1, along with $BaCoS_2$ lattice constants for comparison.

The EDS spectra all displayed K-line peaks that are the signature of potassium, and the semiquantitative results indicate that there is some potassium present in these crystals. Taking the average of about 15 measured regions on surfaces from several crystals, the standardless analysis indicates a potassium concentration of 0.07(3). The indicated standard deviation represents only statistical variation between the 15 measurements. This value is much smaller than the nominal *x* of 0.20, suggesting that a majority of the potassium is not present in the single crystals.

For the room-temperature X-ray data, single-crystal structure refinements were attempted assuming partial K substitution for Ba. The differences between refinements were very small, with the thermal ellipsoids improving upon introduction of K. These differences, however, are not outside of estimated standard deviations. Thus, the K content cannot be reliable determined by X-ray diffraction. However, since potassium is seen in EDS, and sample properties are different from $BaCoS_2$, we feel confident that there is some substitution at the level of $x < 0.07$. Data collection and refinement parameters for the K-disorder model is given in Table 2. The fractional coordinates are presented in Table 3, along with anisotropic thermal parameters in Table 4. Selected bond distances and angles are provided in Table 5.

Table 2. Crystal and Structure Refinement Data for $K_xBa_{1-x}CoS_2$

Crystal Parameters	
empirical formula	$Ba_{0.98}CoK_{0.02}S_2$
formula weight	258.92
crystal system	tetragonal
space group (No.)	*P*4/*nmm* (No. 129)
Z	2
a, Å[a]	4.5565(4)
c, Å	8.9566(12)
volume, Å^3	185.95(3)
ρ_{calc}, mg/m^3	4.624
crystal dimens, mm	0.24 × 0.16 × 0.12
temperature, °C	25
Measurement of Intensity Data and Structure Refinement	
diffractometer	Siemens SMART
radiation, λ, Å	Mo, 0.710 73
2θ range for data collection (deg)	3−56
limiting indices	$-5 \le h \le 5$ $-4 \le k \le 5$ $-7 \le l \le 11$
total reflections	916
independent reflections	164 [R(int) = 0.0287]
no. of observed data	160 ($I > 2\sigma(I)$)
no. of parameters varied	14
μ, mm^{-1}	15.697
absorption correction	empirical (SADABS)
range of trans. factors	0.525−0.928
$R_1(F_o)$, $wR_2(F_o^2)$ %, ($I > 2\sigma(I)$)[b]	1.93, 4.17
$R_1(F_o)$, $wR_2(F_o^2)$ %, all data	2.03, 4.20
goodness-of-fit on F^2	1.266
extinction coefficient	0.061(5)
max and min diff peak, e$^-$/Å^3	0.676 and −0.695
mean shift/esd	0.000

[a] It has been noted that the integration program SAINT produces cell constant errors that are unreasonably small, since systematic error is not included. More reasonable errors might be estimated at 10× the listed values. [b] $R_1 = (S||F_o| - |F_c||)/S|F_o|$, $wR_2 = [S[w(F_o^2 - F_c^2)^2]/S[w(F_o^2)^2]]^{1/2}$, where $w = 1/[\sigma^2(F_0^2) + (aP)^2 + bP]$ and $P = [f(\text{maximum of 0 or } F_o^2) + (1 - f)F_c^2]$.

Table 3. Atomic Coordinates and Equivalent Isotropic Displacement Parameters (Å^2 × 10^3) for $K_xBa_{1-x}CoS_2$[a]

	x	*y*	*z*	*U*(eq)
Ba(1), K(1)	1/4	1/4	0.8039(1)	14(1)
Co(1)	1/4	1/4	0.4069(1)	16(1)
S(1)	1/4	1/4	0.1520(2)	14(1)
S(2)	−1/4	1/4	1/2	28(1)

[a] *U*(eq) is defined as one-third of the trace of the orthogonalized U_{ij} tensor.

While cooling the crystal to 103 K, preliminary lattice parameters were obtained and are shown together with cell volumes in Figure 3. The crystal symmetry appears to reduce to orthorhombic by 243 K, with the cell volume doubling. In the transition region (153 and 123 K), the unit cell is triclinic, and the cell volumes of about 410

Table 4. Anisotropic Displacement Parameters (Å² × 10³) for $K_xBa_{1-x}CoS_2$[a]

	U_{11}	U_{22}	U_{33}	U_{23}	U_{13}	U_{12}
Ba(1), K(1)	16(1)	16(1)	10(1)	0	0	0
Co(1)	20(1)	20(1)	8(1)	0	0	0
S(1)	18(1)	18(1)	7(1)	0	0	0
S(2)	32(1)	32(1)	19(1)	0	0	0

[a] The anisotropic displacement factor exponent takes the form $-2\pi^2[h^2a^{*2}U_{11} + ... + 2hka^*b^*U_{12}]$.

Table 5. Selected Bond Distances (Å) and Angles (deg) of $K_xBa_{1-x}CoS_2$

K,Ba(1)−S(1)	3.118(2)
K,Ba(1)−S(1) × 4	3.2461(4)
K,Ba(1)−S(2) × 4	3.5493(5)
Co(1)−S(1)	2.283(2)
Co(1)−S(2) × 4	2.4261(4)
S(1)−K,Ba(1)−S(1)	83.00(3)
S(1)−K,Ba(1)−S(1)	166.00(7)
S(1)−K,Ba(1)−S(1)	89.149(9)
S(1)−K,Ba(1)−S(2)	140.067(7)
S(1)−K,Ba(1)−S(2)	122.95(3)
S(1)−K,Ba(1)−S(2)	69.08(3)
S(2)−K,Ba(1)−S(2)	53.987(8)
S(2)−K,Ba(1)−S(2)	79.866(14)
S(1)−Co(1)-S(2)	110.11(3)
S(2)−Co(1)-S(2)	83.21(2)
S(2)−Co(1)-S(2)	139.79(5)

Å³ are not multiples of the room-temperature volume. By 100 K, the reflections index to a triclinic cell whose volume is 4 times that of the room-temperature cell. A full data set, with conditions similar to that taken at room temperature, was collected at 183 K, where the preliminary unit cell appears to be orthorhombic. Unfortunately, a feasible atomic model could not be determined to refine the structure. The crystal was again taken up to room temperature, upon which another full data set was taken. The refined structure and lattice parameters showed no deviations from the previous data set, so this transformation appears to be reversible.

The room-temperature resistivity obtained from the van der Pauw measurement was 0.025(4) Ω cm, a value consistent with measurements done on previous crystals. The temperature dependence of the electrical resistivity (Figure 4) displays a phase transition, with a maximum in the resistivity occurring at 164 K. Below this transition, the resistivity drops an order of magnitude and decreases in value down to 4.2 K. Upon warming, significant thermal hysteresis is observed, with a resistivity maximum at 208 K. In the transition region, where the magnitude of the electrical resistivity is changing significantly, the data are not smooth. Looking closely at the data from 100 to 200 K, several "steps" may be identified in both warming and cooling data.

Figure 5 displays the susceptibility data collected by SQUID magnetometry. Around 260 K, the data display a broad rollover, possibly indicative of a second-order phase transition. The data also show another phase transition with hysteresis in the temperature region between 120 and 220 K, with a transition width of 20 K. At low temperatures, the susceptibility value increases to about 8×10^{-6} emu/g at 2 K.

At room temperature, the sample portrayed a slightly negative slope in the χ vs $1/H$ data, with a difference in χ over the one tesla range of about 1×10^{-6} emu/g. At 2 K, the susceptibility showed a positive slope in the field dependence, which could be indicative of weak ferromagnetic contamination, presumably due to impurities.

The low-temperature susceptibility data were fit to the Curie−Weiss law

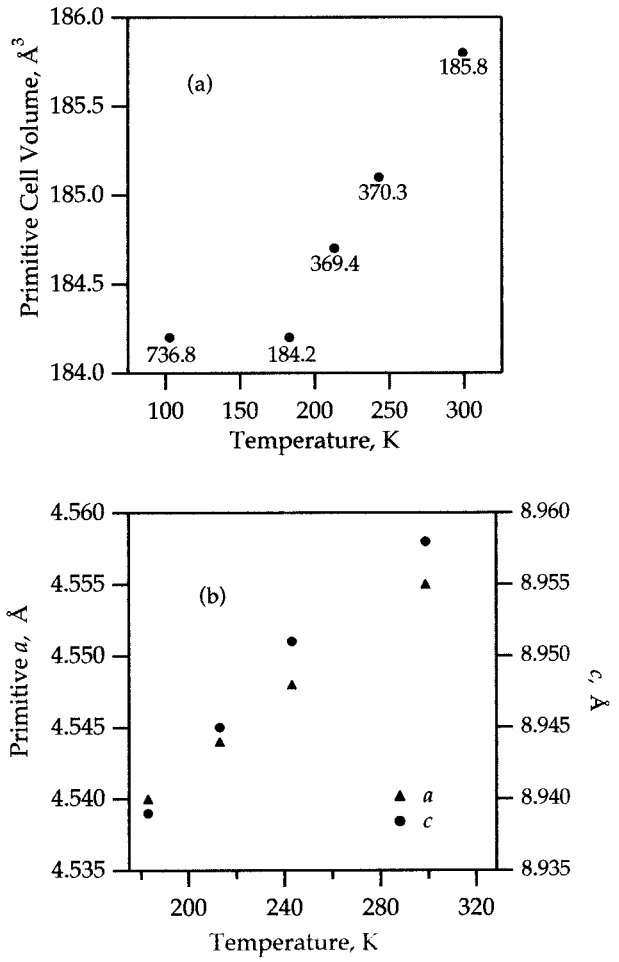

Figure 3. Single-crystal lattice constants and volume as a function of temperature. In (a), actual cell volumes are indicated next to the markers; note that the doubled, orthorhombic cells are metrically equivalent to the primitive monoclinic cells. (b) illustrates the primitive cell constants as a function of temperature above the transition.

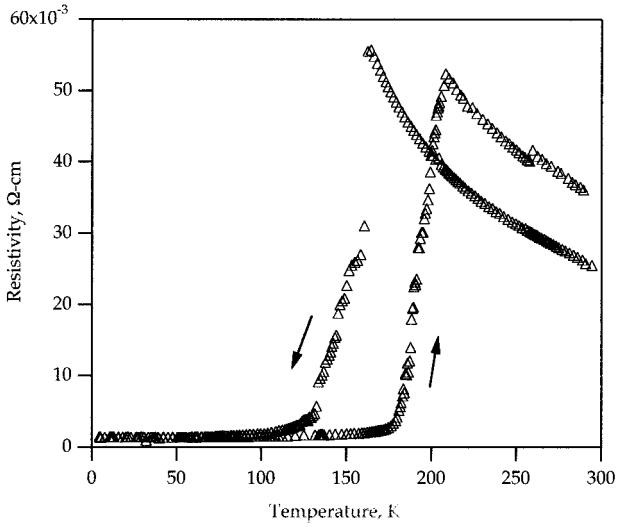

Figure 4. Van der Pauw resistivity vs temperature for $K_xBa_{1-x}CoS_2$ crystal.

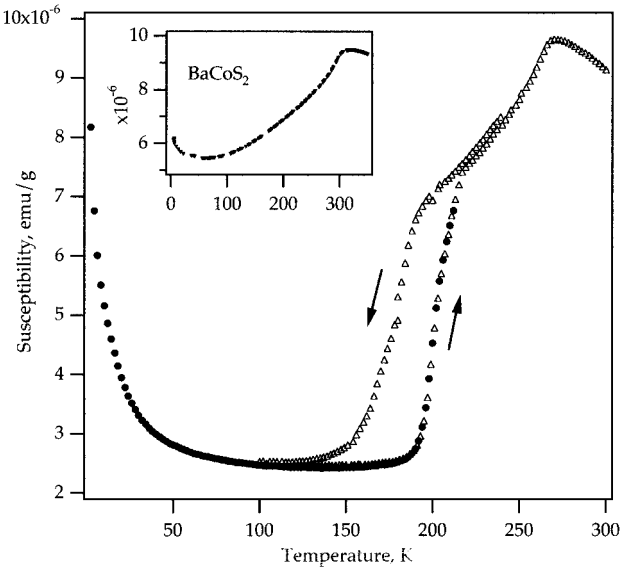

Figure 5. Magnetic susceptibility vs temperature for $K_xBa_{1-x}CoS_2$ crystals. Inset illustrates the magnetic data for undoped, polycrystalline $BaCoS_2$.

$$\chi = \chi_0 + C/(T + \theta)$$

over 2−150 K, which yielded constants of $\chi_0 = 2.08(7) \times 10^{-6}$ emu/g, $C_g = 4.2(6) \times 10^{-5}$ emu K/g, and $\theta = 4(2)$ K, with an effective magnetic moment, μ_{eff}, of 0.290 μ_B. Assuming that the experimental moment is due only to spin $^1/_2$ impurities, the calculated impurity concentration is 2.8%. If spin 2 and $g = 2$ (e.g., paramagnetic Fe) is assumed for the alleged impurities, then the calculated concentration is 0.4%.

Discussion

Because of the similarities between single-crystal refinements, X-ray data do little to confirm the presence of potassium in these crystals. The cell parameters from the single-crystal work are reasonably close to those obtained from powder diffraction, within about 3σ, with a corresponding volume difference of 0.5%. This small difference may reflect an inhomogeneity between crystals. Compared to $BaCoS_2$ single-crystal values (Table 1), both a_{crys} and c_{crys} change by 0.2%, with a decreasing by 0.01 Å, c increasing by 0.015 Å, and V decreasing by 0.3%; the corresponding differences for a_{pow} and c_{pow} are just 0.5% and 0.1%, respectively, with a cell volume reduction of 0.9%.

Because a reasonable structure could not be obtained for the low-temperature X-ray data, no definite conclusions can be drawn concerning the changes in lattice symmetry upon cooling. These changes do correlate well with the magnetic and electrical data, however, and therefore suggest that whatever is occurring with the properties is structural in origin.

As mentioned previously,[3] tetragonal crystals of $BaCoS_2$ were the minority phase in the mostly orthorhombic powder. For all the samples studied, the monoclinic distortion that is the signature of $BaCoS_2$ is no longer present. This consistent symmetry change, evidenced in X-ray diffraction by the absence of splitting in the 11*l* reflections, is strong evidence that there is some degree of substitution. However, the amount of potassium present in the crystals is much smaller than the nominal composition of $x \approx 0.20$. X-ray diffraction, microprobe (EDS) studies, and physical property measurements offer compelling evidence that the crystals are doped.

The electrical and magnetic temperature data both indicate some significant changes taking place with substitution. Polycrystalline $BaCoS_2$ has not displayed hysteretic transitions such as those seen in this study; this fact offers more indirect evidence that the composition of the doped material is different than $BaCoS_2$. Resistivity measurements on polycrystalline, impure $K_xBa_{1-x}CoS_2$ powders also reproducibly displayed this transition. The "jumpiness" of the data around the transition—possibly due to differences between grains in the crystal and not observed in measurements of the polycrystalline material—cannot be adequately explained without a careful study of the grains and their interactions throughout the transition.

At room temperature, the magnitude of the electrical resistivity combined with the temperature dependence suggests semiconducting behavior. The high-temperature data was fit to an Arrhenius expression, $\rho = \rho_0 \exp(E_{act}/k_BT)$, which yielded an activation energy E_{act} of 0.02 eV, smaller than that of $BaCoS_2$ by a factor of 4.[1] The low-temperature data, with a resistivity on the order of 10^{-3} Ω cm and a positive slope, suggests behavior consistent with a poor metal. In comparison, $BaNiS_2$ has a resistivity of 10^{-3}−10^{-4} Ω cm, with a fairly weak temperature dependence.[4,16] This insulator−metal resistivity behavior is reminiscent of that seen in the $Ba(Co,Ni)S_{2-y}$ phases.[7] The main distinction is that the drop in resistivity for the (Co,Ni) alloys is over a few orders of magnitude from a higher initial resistivity, rather than just the 1 order of magnitude observed here.

The magnetic susceptibility data suggest a second-order transition near 260 K. In $BaCoS_2$, an almost identical transition at 310 K has been confirmed to be due to an antiferromagnetic ordering.[3,5] Below 200 K, the structure begins to contract, which may increase interaction between the ordering Co^{2+} moments. Upon contraction, however, the Co d and S p orbitals would overlap more than they do at high temperatures, perhaps enough to lift the Mott condition and enable metallic behavior. However, this is the opposite of what is observed in many other metal−insulator transitions, where the metallic state is at high temperatures. The value of the susceptibility at low temperature is around 2×10^{-6} emu/g after subtracting a Curie contribution due to impurities or defects. The low-temperature behavior of the susceptibility is most likely Pauli paramagnetic.

Conclusions

The preparation technique of using closed vitreous carbon could prove to be extremely useful in syntheses which require high temperatures and use of substances that react with quartz and other containers. However, its use may be limited to materials with relatively small vapor pressures.

$K_xBa_{1-x}CoS_2$, at substitution levels of several percent, is structurally quite different from its parent phase

(16) Gelabert, M. C.; Drinkwater, D.; DiSalvo, F. J. *J. Alloys, Compd.* **1996**, *241*, 89.

$BaCoS_2$. The tetragonal symmetry that the substituted phase possesses is a clear indication that the product is modified from orthorhombic $BaCoS_2$. The metal−insulator transition observed in the electrical resistivity as a function of temperature correlates well with the first-order transition in magnetic susceptibility. These measurements, combined with low-temperature X-ray diffraction, indicate significant structural changes taking place throughout the transition, with symmetry reduction and superlattice formation.

The family of compounds containing $BaCoS_2$ offers a rich chemistry combined with interesting transport and magnetic phenomena; this combination is a crucial element in the process of understanding more precisely the various relationships between structure and properties. Further study of Mott insulators, particularly those with low dimension, will continue to provide useful data for the knowledge base of materials chemistry.

Acknowledgment. M.C.G. would like to acknowledge G. R. Kowach and R. C. Haushalter of NEC Research Institute, Princeton, NJ, for use of the SQUID magnetometer, and D. Venkataraman for insightful crystallographic discussion. This work was supported by the U.S. Department of Energy Grant number DE-FG02-87ER45298.

CM970604A